

# Dark-ages Reionization and Galaxy Formation Simulation XX. The Ly $\alpha$ IGM transmission properties and environment of bright galaxies during the Epoch of Reionization

Yuxiang Qin<sup>1,2,3\*</sup>, J. Stuart B. Wyithe<sup>1,2</sup>, Pascal A. Oesch<sup>4,5</sup>, Garth D. Illingworth<sup>6</sup>,  
Ecaterina Leonova<sup>4</sup>, Simon J. Mutch<sup>1,2</sup> and Rohan P. Naidu<sup>7</sup>

<sup>1</sup>*School of Physics, University of Melbourne, Parkville, VIC 3010, Australia*

<sup>2</sup>*ARC Centre of Excellence for All Sky Astrophysics in 3 Dimensions (ASTRO 3D)*

<sup>3</sup>*Scuola Normale Superiore, Piazza dei Cavalieri 7, I-56126 Pisa, Italy*

<sup>4</sup>*Department of Astronomy, University of Geneva, Chemin Pegasi 51, 1290 Versoix, Switzerland*

<sup>5</sup>*Cosmic Dawn Center (DAWN), Niels Bohr Institute, University of Copenhagen, Jagtvej 128, København N, DK-2200, Denmark*

<sup>6</sup>*Department of Astronomy and Astrophysics, UCO/Lick Observatory, University of California, Santa Cruz, CA 95064, USA*

<sup>7</sup>*Center for Astrophysics | Harvard & Smithsonian, 60 Garden Street, Cambridge, MA 02138, USA*

10 August 2021

## ABSTRACT

The highly neutral inter-galactic medium (IGM) during the Epoch of Reionization (EoR) is expected to suppress Ly $\alpha$  emission with damping-wing absorption, causing nearly no Ly $\alpha$  detection from star-forming galaxies at  $z \sim 8$ . However, spectroscopic observations of the 4 brightest galaxies ( $H_{160} \sim 25$  mag) at these redshifts do reveal prominent Ly $\alpha$  line, suggesting locally ionised IGM. In this paper, we explore the Ly $\alpha$  IGM transmission and environment of bright galaxies during the EoR using the Meraxes semi-analytic model. We find brighter galaxies to be less affected by damping-wing absorption as they are effective at ionizing surrounding neutral hydrogen. Specifically, the brightest sources ( $H_{160} \lesssim 25.5$  mag) lie in the largest ionized regions in our simulation, and have low attenuation of their Ly $\alpha$  from the IGM (optical depth  $< 1$ ). Fainter galaxies ( $25.5 \text{ mag} < H_{160} < 27.5$  mag) have transmission that depends on UV luminosity, leading to a lower incidence of Ly $\alpha$  detection at fainter magnitudes. This luminosity-dependent attenuation explains why Ly $\alpha$  has only been observed in the brightest galaxies at  $z \sim 8$ . Follow-up observations have revealed counterparts in the vicinity of these confirmed  $z \sim 8$  Ly $\alpha$  emitters. The environments of our modelled analogues agree with these observations in the number of nearby galaxies, which is a good indicator of whether Ly $\alpha$  can be detected among fainter galaxies. At the current observational limit, galaxies with  $\geq 2$ –5 neighbours within  $2' \times 2'$  are  $\sim 2$ –3 times more likely to show Ly $\alpha$  emission. *JWST* will discover an order of magnitude more neighbours, revealing  $\gtrsim 50$  galaxies in the largest ionizing bubbles and facilitating direct study of reionization morphology.

**Key words:** cosmology: theory – dark ages, reionization, first stars – diffuse radiation – early Universe – galaxies: high-redshift – intergalactic medium

## 1 INTRODUCTION

The transmission of Lyman- $\alpha$  (Ly $\alpha$ ) photons has played a significant role in observational studies of reionization due to its highly resonant nature in neutral hydrogen, which provides a direct probe of the ionization state of the intergalactic medium (IGM). Toward the end of reionization, the large-scale HI distribution has been studied with the

Ly $\alpha$  forest along the line of sight towards bright background quasars (Bolton et al. 2010; Lidz et al. 2010; Lee et al. 2015; Puchwein et al. 2015; Bolton et al. 2017; Gaikwad et al. 2020). For instance, by counting the zero-flux pixels on quasar spectra, McGreer et al. (2015) concludes that the average neutral hydrogen fraction ( $x_{\text{HI}}$ ) at  $z \sim 5.9$  should be lower than 6 – 11 per cent ( $1\sigma$ ; see also upcoming works by Campo et al., in prep. and Jin et al., in prep.). However, individual sight-lines seem to suggest that large chunks ( $> 160 \text{ cMpc}$ ) of residual HI still exist even at  $z < 6$  (Becker

\* E-mail: Yuxiang.L.Qin@gmail.com

et al. 2015; Zhu et al., in prep.), requiring late reionization and/or that the underlying accountable sources possess unusual ionizing properties (e.g. D’Aloisio et al. 2015, 2018; Chardin et al. 2015, 2017; Davies & Furlanetto 2016; Keating et al. 2018, 2020; Kulkarni et al. 2019; Meiksin 2020; Nasir & D’Aloisio 2020; Qin et al. 2021).

Damping-wing absorption of Ly $\alpha$  emission lines of quasars (in particular the red side of the line center on a quasar spectrum) also facilitates estimates of  $x_{\text{HI}}$  during the epoch of reionization (EoR). This is done by directly comparing the observed flux to the intrinsic flux inferred from low-redshift analogues using continuum and metal lines. For instance, among some of the 9 quasars discovered at  $z > 7$  to date (Bosman 2020 and reference therein), high-quality spectra have enabled direct measurement of the neutral hydrogen, ranging from  $x_{\text{HI}} \sim 10\%$  to  $80\%$  (Mortlock et al. 2011; Greig et al. 2017, 2019; Bañados et al. 2018; Davies et al. 2018; Wang et al. 2020; Yang et al. 2020).

High-redshift star-forming galaxies that have detectable Ly $\alpha$  emission (e.g. with a equivalent width larger than  $25\text{\AA}$ ) are referred to as Ly $\alpha$  emitting galaxies (LAEs). The incidence of LAEs has also been used to determine the neutral fraction (Mason et al. 2018a,b). This is because Ly $\alpha$  detection during the EoR could provide evidence for whether galaxies sit in large ionized bubbles, so that their Ly $\alpha$  photons are redshifted deep into the damping wing, and are therefore less attenuated by the intergalactic HI (Dijkstra 2014). As the Universe becomes more neutral, observations have shown a rapidly decreasing fraction of LAEs among Lyman break galaxies (LBGs) from  $z = 6$  to  $8$  (Fontana et al. 2010; Stark et al. 2010; Ono et al. 2012; Treu et al. 2013; Schenker et al. 2014; Hoag et al. 2019).

However, despite the increasing neutral fraction in the high-redshift Universe, prominent Ly $\alpha$  lines in some of the brightest sources have been observed even out to  $z \sim 9$  with a much higher detection rate of Ly $\alpha$  emission than expected. In particular, the 4 most luminous galaxies ( $H_{160} \sim 25$  mag) in CANDELS have all been spectroscopically confirmed by Keck as LAEs (Oesch et al. 2015; Zitrin et al. 2015; Roberts-Borsani et al. 2016; Stark et al. 2017; see also Tilvi et al. 2020). In contrast, when targeting relatively fainter galaxies, no Ly $\alpha$  emission was detected at  $z \sim 8$  while  $p(\text{Ly}\alpha)$  was found to be  $< 2\%$  and  $< 15\%$  at  $z \sim 7.5$  and  $7$ , respectively (Schenker et al. 2014; Hoag et al. 2019). Similarly, more recent larger spectroscopic samples of Ly $\alpha$  emission among high-redshift, bright galaxies find  $p(\text{Ly}\alpha)$  varying between  $20\%$  and  $50\%$  at  $6 \lesssim z \leq 9$  (Jung et al. 2020; Endsley et al. 2021; Laporte et al. 2021). Apart from possibly having higher intrinsic Ly $\alpha$  emission due to recent star formation, these brightest galaxies are likely located in more overdense regions, and may be surrounded by a larger number of star-forming galaxies producing a more transparent IGM (Wyithe & Loeb 2005).

In this work, we use a semi-analytic galaxy-formation model to explore the Ly $\alpha$  IGM transmission properties and environment of bright galaxies during the EoR. We focus on both the brightest galaxies, which are analogous to those observed at  $z \sim 8$ , as well as relatively fainter galaxies, including those that can be considered promising candidates for the *James Webb Space Telescope* (*JWST*; e.g. Malkan et al. 2021; Naidu et al. 2021; Oesch et al. 2021). Our semi-analytic model (SAM) follows a number of astrophysical pro-

cesses of galaxy formation and self-consistently calculates photon-heating feedback from reionization as well as recombination in HII regions. The model has been shown to successfully reproduce a large number of observables (Mutch et al. 2016; Liu et al. 2016; Qin et al. 2017b) including galaxy (Bouwens et al. 2015, 2016) and quasar UV luminosity functions (LFs; Wolf et al. 2003; Bongiorno et al. 2007; Croom et al. 2009; Glikman et al. 2011; Masters et al. 2012; Palanque-DeLabrouille et al. 2013) in addition to the inferred EoR history from the cosmic microwave background (CMB; Planck Collaboration et al. 2020, see also Qin et al. 2020).

This paper is organized as follows. We provide a brief review of our model as well as the newly implemented calculation of Ly $\alpha$  damping-wing absorption in Section 2. We present our results including the strategy for hunting LAEs in Section 3 before concluding in Section 4. In this work, we set the following cosmological parameters based on the *Planck* 2015 results ( $\Omega_{\text{m}}, \Omega_{\text{b}}, \Omega_{\Lambda}, h, \sigma_8, n_s = 0.308, 0.0484, 0.692, 0.678, 0.815, 0.968$ ; Planck Collaboration et al. 2016).

## 2 MODELING HIGH-REDSHIFT GALAXY PROPERTIES AND REIONIZATION

We use the MERAXES SAM (Mutch et al. 2016; Qin et al. 2017b) from the DRAGONS (Dark-ages Reionization And Galaxy formation Observables from Numerical Simulations) program, which is coupled to a parent  $N$ -body simulation (Poole et al. 2016) providing dark matter halo properties from  $z = 35$  to  $2$ . The upper left panel of Fig. 1 illustrates the matter density at  $z = 8$  in our simulation volume. With a mass resolution of  $\sim 4 \times 10^6 M_{\odot}$  and a box size of  $100\text{cMpc}$ , we are able to properly sample low-mass halos down to the atomic cooling threshold and capture massive galaxies of  $\sim 7 \times 10^{11} M_{\odot}$  at  $z = 8$ . These allow us to resolve faint galaxies that are responsible for reionization (Liu et al. 2016) and study galaxies as bright as  $M_{1600} \sim -22$  mag at  $z = 11$  (Mutch et al. 2016) or  $H_{160} = 24.5$  mag (i.e. the *Hubble Space Telescope* or *HST* F160W band) at  $z = 8$ . While we refer interested readers for detailed semi-analytic prescriptions of galaxy formation to Mutch et al. (2016) and Qin et al. (2017b), some basic characteristics of our model are presented below.

### 2.1 High-redshift galaxies

MERAXES evaluates the accretion and cooling of gas, stellar evolution and feedback, growth of supermassive blackholes and their impact on galaxy formation, as well as other environmental influences such as mergers and photo-heating from reionization. We also consider dust attenuation and forward model the observed galaxy and quasar UV magnitudes (e.g.  $H_{160}$ ). These allow us to adjust our model parameters in order to match the predicted observables with existing measurements during the EoR. These include the stellar mass function, UV LFs of LBGs and high-redshift quasars, ionizing emissivities, and the Thomson scattering optical depth of the CMB photons. In this work, we use the galaxy catalogue generated by the fiducial model presented in Qin et al. (2017b). As an illustration, Fig. 1 populates

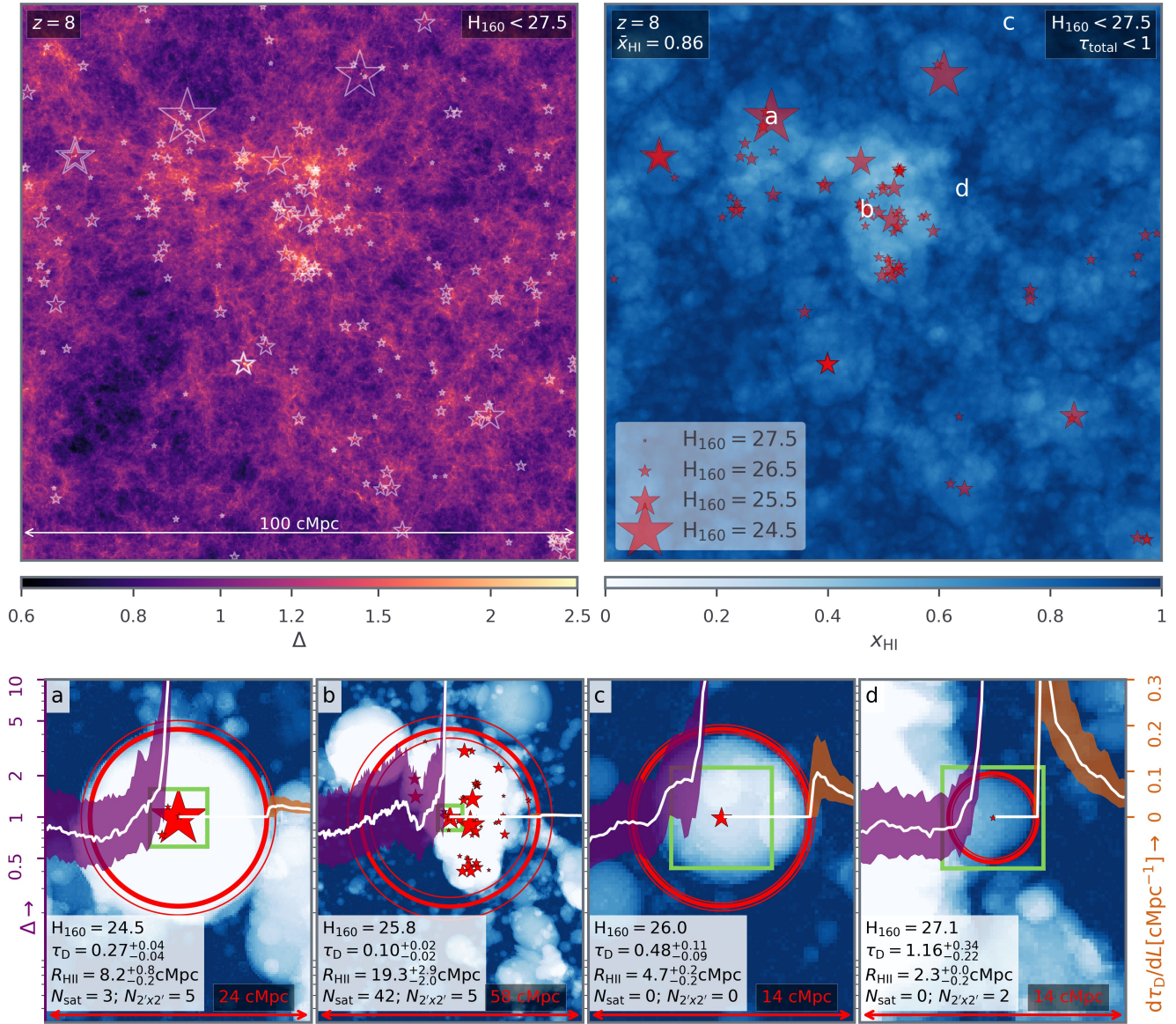


**Figure 1.** *Upper panels:* overdensity ( $\Delta$ ) and neutral hydrogen fraction ( $x_{\text{HI}}$ ) of the entire simulation volume at  $z=8$  (projected with a depth of 100cMpc). In the density plot, galaxies brighter than  $H_{160}=27.5$  mag are indicated using star symbols with increasing sizes representing higher luminosities. In the HI plot, only UV-bright, Ly $\alpha$ -transparent (i.e.  $\tau_{\text{total}} < 1$ ) galaxies are shown and the location of four example galaxies (a, b, c, d; see more in Section 2.4) are indicated. *Bottom panels:* highlights of four bright galaxies (zoom-in projection with a depth of 10cMpc for  $x_{\text{HI}}$  and bright galaxies within the same HII bubble). Radial profiles of  $\Delta$  (purple; left-hand side) and the damping-wing optical depth gradient ( $d\tau_{\text{D}}/dL$ ; yellow; right-hand side) are shown with their medians and uncertainties ([16, 84] percentiles) among 500 random sight-lines highlighted with white solid curves and colored regions, respectively. Their vertical ranges are presented on the left- and right-hand side of the bottom panels, separately. Presented in the lower left corner of each sub-panel are the target galaxy luminosity, damping-wing optical depth and bubble radius, followed by the number of neighbouring bright galaxies ( $H_{160} < 27.5$  mag) within the HII bubble (mean radius indicated by thick red circles with the thin ones for uncertainties) and that within a *HST* WFC3 FoV ( $2' \times 2'$ ; 2D projection with  $\Delta z \sim 1$ ; green square).

the modelled bright galaxies ( $H_{160} < 27.5$  mag; i.e. the current CANDELS DEEP  $5\sigma$  depth, see e.g. Roberts-Borsani et al. 2016) in the density plot with larger star symbols indicating higher luminosities.

Modelling the intrinsic Ly $\alpha$  profile of individual galaxies (Verhamme et al. 2006; Le Delliou et al. 2006; Dijkstra et al. 2007; Zheng et al. 2010; Song et al. 2020; Garel et al. 2021) is deferred to future work. Here, we assume all star-forming galaxies during the EoR are effective at producing

Ly $\alpha$  photons and their detectability in Ly $\alpha$  is solely determined by neutral hydrogen present along the line of sight (e.g. Gronke et al. 2020; see more discussion in Section 2.3).

## 2.2 Ionizing the IGM

To evaluate the IGM ionization state, MERAXES couples its UV ionizing photon source (i.e. star-forming galaxies and quasars) model with 21cmFAST (Mesinger et al. 2011; Mur-

ray et al. 2020). We divide the simulation volume into  $N=512^3$  cells having an equal length of  $L=0.195\text{cMpc}$ . With an excursion-set algorithm (Furlanetto et al. 2004), we compare the ionizing photon budget to the number of present neutral hydrogen atoms (including those recombined after ionization) and estimate the neutral hydrogen fraction ( $x_{\text{HI}}$ ) in each cell.

The model used in this work has a predicted EoR history consistent with the latest *Planck* results (Planck Collaboration et al. 2016, 2020; Qin et al. 2020). It is predominantly driven by UV ionizing photons emitted by stars in faint galaxies (Liu et al. 2016) with supermassive blackholes having an insignificant contribution to the overall reionization (e.g.  $\lesssim 5$  per cent of the ionizing production rate at  $z \geq 7$ ; Qin et al. 2017b). The only regions of ionizing background dominated by luminous AGN are in their immediate environment (Qin et al. 2017a). The upper right panel of Fig. 1 illustrates the modelled ionization field at  $z = 8$  where the volume-averaged neutral hydrogen fraction is  $\bar{x}_{\text{HI}} = 0.86$ . We see reionization (anti-)correlates with underlying densities and brighter galaxies, in general, are located in larger HII bubbles. We also confirm that, in these star-forming galaxies, the central supermassive black holes have a negligible role in ionizing the surrounding IGM.

### 2.3 Ly $\alpha$ damping-wing absorption

We compute the Ly $\alpha$  optical depth in each cell based on

$$\tau_\alpha = Ln_{\text{H},0}x_{\text{HI}}\Delta(1+z)^2\sigma_\alpha, \quad (1)$$

where  $L$ ,  $n_{\text{H},0}$  and  $\Delta$  are the pixel length, the cosmic mean of the comoving hydrogen number density and its local overdensity in each cell, while

$$\sigma_\alpha \left( x \equiv \frac{\lambda_\alpha}{\lambda} \right) = \frac{3\lambda_\alpha^2}{8\pi} \frac{x^4}{1/4x^6 + (1-x)^2(2\pi c/\lambda_\alpha\Lambda)^2} \quad (2)$$

corresponds to the Ly $\alpha$  scattering cross section in HI redwards of the line centre (i.e.  $x < 1$ ; Miralda-Escudé 1998) with  $c$  and  $\Lambda = 6.25 \times 10^8 \text{s}^{-1}$  representing the speed of light and the decay constant for the Ly $\alpha$  resonance. From these two equations, we see that damping-wing absorption increases towards higher redshifts [ $\tau_\alpha \propto (1+z)^2$ ] and drops significantly ( $\sigma_\alpha \propto \lambda^{-4}$ ; i.e. Rayleigh-type scattering) at distances further from the line center [i.e.  $x \ll 1 - \Lambda\lambda_\alpha/(2\pi c)$ ]. Therefore, we ignore damping-wing absorption at distances longer than our box length (i.e. 100cMpc) and estimate the total optical depth as  $\tau_{\text{D}} = \sum_{i=0}^{\sqrt[3]{N}-1} \tau_{\alpha,i}$ . Here,  $\tau_{\alpha,i}$  represents the optical depth in the  $i$ th cell away from the source along a sight-line where Ly $\alpha$  has shifted to  $\lambda = \lambda_\alpha [1 + (V_{\text{offset}} + iLH)/c]$  with  $V_{\text{offset}}$  and  $H(z)$  representing the velocity offset of the intrinsic Ly $\alpha$  line and the Hubble parameter at  $z$ . Note that, for each bright galaxy, we randomly select 500 sight-lines and estimate the bubble size<sup>1</sup> and  $\tau_{\text{D}}$  as well as their associated uncertainties by taking the median and [16, 84] percentiles.

There are an increasing number of observed LAEs presenting a velocity offset between the Ly $\alpha$  emission peak and the systemic redshift up to  $V_{\text{offset}} \sim 1000 \text{km s}^{-1}$ , as well as

<sup>1</sup> For each target galaxy, we consider its distance to the first cell on the sight-line with an ionization phase transition (i.e.  $x_{\text{HI}} \geq 0.9$  in this work) as its bubble radius.

a possible correlation (using large samples at low redshifts) showing higher  $V_{\text{offset}}$  with increasing galaxy UV luminosities (Erb et al. 2014; Muzahid et al. 2020; Endsley et al., in prep.). This could increase the Ly $\alpha$  transmission in the IGM for brighter galaxies (Dijkstra et al. 2007; Choudhury et al. 2015; Mason et al. 2018a,b). However, when splitting low-redshift LAEs by their UV magnitudes, we see the opposite with more luminous galaxies showing a lower fraction of LAEs (e.g. Schenker et al. 2014; Garel et al. 2015), possibly due to a reduced Ly $\alpha$  escape fraction in deeper gravitational potentials (Oyarzún et al. 2017; Yang et al. 2017; Hassan & Gronke 2021). As current measurements are still inconclusive and limited by the small LAE sample, particularly at higher redshifts, we do not consider the intrinsic line intensity, offset or escape fraction of Ly $\alpha$ . Since the targets in this work are those mostly sitting in large HII bubbles, we also expect them to be less affected by  $V_{\text{offset}}$ . Based on these, we treat the detectability of a LAE governed primarily by its IGM transmission.

It is worth noting that fully ionized regions do not contribute to the total damping-wing optical depth according to equation (1) as  $x_{\text{HI}}=0$ . However, to account for resonant absorption by residual neutral hydrogen inside the ionized region (Mesinger et al. 2015; Park et al. 2021), we follow previous work (e.g. Mason et al. 2018b) and assume all flux bluer than the circular velocity of the host halo becomes attenuated. This leads to a factor of 2 further reduction to the Ly $\alpha$  transmission ( $\mathcal{T}$ ) so that

$$\mathcal{T} \equiv \exp(-\tau_{\text{total}}) \equiv \exp(-\tau_{\text{D}} - \tau_{\text{HII}}) = 0.5 \exp(-\tau_{\text{D}}). \quad (3)$$

This results in an optical depth inside HII regions of  $\tau_{\text{HII}} \sim 0.69$  while  $\tau_{\text{total}}$  in equation (3) represents the total optical depth.

In this work, we consider *galaxies with  $\tau_{\text{total}}$  larger (or lower) than 1 as highly attenuated (or transparent) LAEs subject to damping-wing absorption in the IGM*. The upper right panel of Fig. 1 shows the location of UV-bright, transparent-LAEs. We see a large fraction (>60%) of UV-bright LBGs are excluded (c.f. the upper left panel of Fig. 1) as they are still too faint and/or isolated from other bright sources to ionize their surrounding neutral hydrogen.

### 2.4 Example LAEs

We highlight four example galaxies in the bottom panels of Fig. 1. These galaxies are, in each case, the brightest galaxy found in their HII bubble. Hence, we also refer to them as the central galaxy and consider the remaining counterparts in the bubble as their satellites<sup>2</sup>. In each sub-panel, we also illustrate the overdensity (purple; left-hand side) and Ly $\alpha$  damping-wing optical depth as in  $d\tau_{\text{D}}/dL$  (yellow; right-hand side) among 500 random sight-lines towards the target galaxy.

<sup>2</sup> As some bubbles are highly non-spherical, e.g. Galaxy b in Fig. 1, there are scenarios where a brighter galaxy, the central of its own HII bubble ( $R_{\text{HII,bright}}$ ), can be considered as a satellite of an other galaxy which is fainter but has a bubble size ( $R_{\text{HII,faint}}$ ) larger than the brighter one. Note that this fainter galaxy is not categorised as a satellite of the brighter one because their separation is longer than  $R_{\text{HII,bright}}$  but shorter than  $R_{\text{HII,fainter}}$

Furthermore, we consider *HST* WFC3 mock images centred at the target galaxies (see the green square; same projected direction as HII) and count the number of neighbouring  $H_{160} < 27.5$  mag galaxies within a field of view (FoV) of  $2' \times 2'$  and a depth of  $\Delta z \sim 1$ . The latter is a conservative choice set by the photometric uncertainty in relevant observations ( $\Delta z \sim \pm 0.1$ – $0.4$ , e.g. Roberts-Borsani et al. 2016; see also Bouwens et al. 2015). Note that as our box length sets the observational depth to be  $\Delta z \sim 0.35$  at  $z=8$ ,  $\sim 3$  times smaller than the desired value, we extend each mock observation with two more randomly selected sight-lines before projection. To account for galaxy evolution, we choose the sight-lines from simulation snapshots at  $z=7.5$  and  $8.5$  separately. These allow us to account for foreground and background galaxies within our FoV due to random alignment, the number of which is  $1 \pm 1$  (median with [16, 84] percentiles). Below, we discuss each of the 4 example galaxies shown in Fig. 1 in turn.

**Galaxy a.** The brightest galaxy in our simulation snapshot with  $H_{160}=24.5$  mag. This galaxy is considered to be an observable LAE with the UV ionizing photons in this area coming predominately from itself and resulting in a Ly $\alpha$  damping-wing optical depth of  $\tau_D \sim 0.27$ . There are also 3 satellite galaxies with  $H_{160} < 27.5$  mag in its HII bubble with a radius of  $R_{\text{HII}} \sim 8$  cMpc. In the mock observation, we expect to find 2 more galaxies randomly aligned in the FoV in addition to the 3 satellites.

**Galaxy b.** A luminous galaxy ( $H_{160}=25.8$  mag) located in one of the largest HII regions in our simulation with  $\tau_D \sim 0.10$ . Centred at this particular galaxy, we obtain a highly non-spherical HII bubble (i.e.  $R_{\text{HII}} \sim 19$  cMpc with a large uncertainty of  $2 - 3$  cMpc). Within a sphere of  $R_{\text{HII}} \sim 19$  cMpc, more than 40 galaxies with  $H_{160} < 27.5$  mag contribute to the local ionizing photon budget and 5 of them are expected in the mock observation (no random alignment). This galaxy has a damping-wing optical depth much smaller than the brightest one (i.e. Galaxy a), suggesting that bright galaxies are more likely to have observable Ly $\alpha$  emission when clustered (Wyithe & Loeb 2005; Trac & Gnedin 2011; Endsley et al. 2021; see also the recent report on a LAE cluster at  $z \sim 7$  by Hu et al. 2021 and an upcoming result from Jung et al., in prep. showing boosted IGM transmission around bright galaxies at  $z > 6$ ).

**Galaxy c.** The brightest galaxy in our simulation that is considered to be an obscured LAE. This galaxy has a similar UV magnitude ( $H_{160}=26$  mag) to Galaxy b, but is located in a much smaller HII bubble ( $\sim 5$  cMpc) and possesses a  $\tau_D$  nearly 4 times larger in the absence of any other bright galaxies in its vicinity. This shows again that, when observing a LAE during the EoR, it is likely to be surrounded by a group of nearby bright galaxies, further emphasizing the importance of the contributions of neighboring, albeit, fainter galaxies.

**Galaxy d.** A highly Ly $\alpha$ -obscured galaxy ( $H_{160}=27.1$  mag). This object is one order of magnitude fainter than Galaxies b and c, and has a bubble size of only  $\sim 2$  cMpc. It resides in the smallest HII bubble among all bright ( $H_{160} < 27.5$  mag) galaxies and possesses a Ly $\alpha$  transmission rate of only  $\sim 15\%$ . This galaxy has only 2 neighbours within the mock image while both are due to random alignment.

### 3 CHARACTERIZING Ly $\alpha$ TRANSMISSION DURING THE EOR

The 4 modelled galaxies presented above demonstrate some of the characteristic Ly $\alpha$  IGM transmission properties among bright LBGs during the EoR. They also clearly present the real and substantial variations in Ly $\alpha$  detectability within a quite modest range of luminosities (factors of a few). In this section, we use the whole modelled high-redshift galaxy population to quantify how reionization impacts Ly $\alpha$  transmission, and provide guidance for searching for ionized bubbles in the heart of the cosmic reionization epoch.

#### 3.1 Correlation of damping wing with the IGM properties

At a given redshift the damping wing optical depth  $\tau_D$ , on average, decreases if the LAE sits inside larger HII bubbles. This is illustrated in the upper left panel of Fig. 2 for galaxies brighter than  $H_{160}=27.5$  mag. Such a  $\mathcal{T} - R_{\text{HII}}$  correlation becomes obvious when the mean density and neutral hydrogen fraction are substituted in equation (1; see the dashed line in the panel). However, as overdense regions are typically the first to become ionized, we also expect to see a positive correlation between the Ly $\alpha$  transmitted fluxes and large-scale<sup>3</sup> overdensities. This is shown in the upper right panel of Fig. 2 where we also observe a much larger scatter compared to the  $\mathcal{T} - R_{\text{HII}}$  relation. When focusing on currently observable galaxies (i.e.  $H_{160} < 27.5$  mag), we see that the obscured LAEs are on average located in HII regions smaller than  $\sim 7$  cMpc at  $z = 8$  and with an overdensity of  $\Delta_{3D} \lesssim 1$ .

#### 3.2 Correlation of damping wing with galaxy properties

The lower-left panel of Fig. 2 shows the relation between galaxy UV luminosity and Ly $\alpha$  transmission. In general, brighter galaxies possess higher Ly $\alpha$  transmission as their UV ionizing luminosities are more effective at ionizing the surrounding IGM and therefore creating larger HII bubbles (Geil et al. 2017; Davies et al. 2021). However, we also see a bimodal distribution in the  $\mathcal{T} - H_{160}$  relation. After separating galaxies according to their luminosities in each HII bubble, we find that the two peaks originate from different galaxy populations. Central galaxies, defined as the brightest galaxy in each bubble, dominate the local ionizing photon budget and therefore have lower  $\tau_D$  with increasing luminosities. However, most galaxies brighter than  $H_{160} \sim 25.5$  mag have a similar level of damping-wing absorption ( $\tau_D \sim 0.27$  or  $\mathcal{T} \sim 0.38$ ) and all of them are transparent in Ly $\alpha$ . This is consistent with the 4 observed bright LBGs showing strong Ly $\alpha$  emission (Oesch et al. 2015; Zitrin et al. 2015; Roberts-Borsani et al. 2016; Stark et al. 2017) and suggests that the brightest, color-selected LBGs are likely to reside in large HII regions (see estimate of the bubble size by Tilvi et al. 2020 for one of the LAEs) as predicted by

<sup>3</sup> A cubic volume of  $150 \text{ cMpc}^3$  is used to show the large-scale density. This choice is somewhat arbitrary with the side length,  $5.3 \text{ cMpc}$  (i.e.  $2'$  at  $z=8$ ), corresponding to a WFC3 field of view.



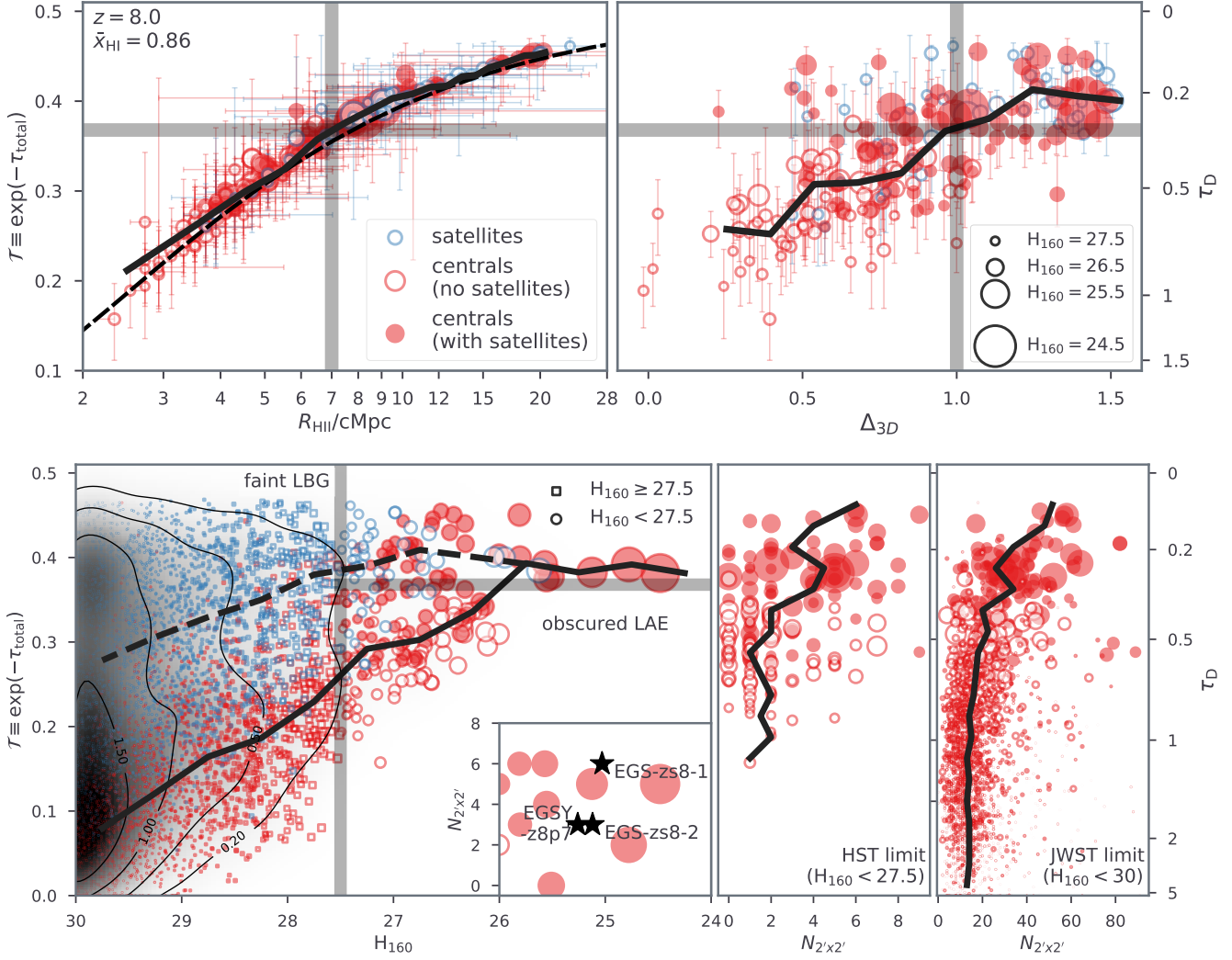


**Figure 2.** *Upper panels:* the Ly $\alpha$  transmission ( $\mathcal{T} \equiv e^{-\tau_{\text{total}}}$ ; left axis) or damping optical depth ( $\tau_{\text{D}}$ ; right axis) as a function of the HII bubble size ( $R_{\text{HII}}$ ; left panel) or overdensity smoothed over a cubic volume of  $150\text{cMpc}^3$  ( $\Delta_{3\text{D}}$ ; right panel) for galaxies brighter than  $H_{160}=27.5$  mag. Central galaxies (i.e. the brightest ones in their HII bubbles) and their satellites (i.e. the remaining galaxies) are shown separately using red and blue colours with increasing circle sizes representing higher luminosities. The errorbar corresponds to [16, 84] percentiles of the transmission and bubble size varying between 500 different random sightlines. The median relation is indicated by the solid curve while the dashed one shows the  $\mathcal{T}-R_{\text{HII}}$  relation at the mean overdensity and neutral hydrogen fraction for comparison.  $\tau_{\text{total}}=1$  is indicated using the horizontal grey stripes with the vertical ones highlighting the corresponding  $R_{\text{HII}}$  and  $\Delta_{3\text{D}}$  on the median relation. *Lower-left panel:* the  $\mathcal{T}-H_{160}$  relation with galaxies fainter than  $H_{160}=27.5$  mag distinguished by the square symbol and further illustrated using a 2D histogram (and contours) for better visualization. The median relations are indicated using the thick solid and dashed black lines for central and satellite galaxies, respectively. The correlation between the number of neighbouring galaxies within a WFC FoV ( $2' \times 2'$ ; 2D projection with  $\Delta z \sim 1$ ) and  $H_{160}$  is shown in the inset for the most luminous centrals. Preliminary estimates (Leonova et al., in prep.) are indicated by the star symbol for 3 objects of the  $z \sim 8$  LAEs (Oesch et al. 2015; Roberts-Borsani et al. 2016; Zitrin et al. 2015). *Lower-right two panels:* the correlation between  $\mathcal{T}$  and the number of neighbours brighter than  $H_{160}=27.5$  or 30 mag (*JWST* limit). In these two panels, galaxies shown are also brighter than the *HST*/*JWST* limit, and the median relations are binned by  $\mathcal{T}$ . Central galaxies having satellites within their bubbles (both are brighter than the *HST* limit) are highlighted with filled circles.

generic inside-out models of reionization. On the other hand, fainter satellite galaxies have their HII bubble size mostly set by the central galaxies. Therefore, we see a horizontal offset towards lower luminosity<sup>4</sup> from the median  $\mathcal{T}-H_{160}$  relation of central galaxies (shown as the solid curve) to that of the satellites (dashed curve). Comparing between the two galaxy

populations, we see that galaxies fainter than  $H_{160} \sim 27.5$  can only be detected in Ly $\alpha$  when they share the same HII bubble as another brighter one.

We showed in Section 2.4 that, despite being more than one magnitude fainter than the brightest galaxy in our simulation (i.e. Galaxy a), Galaxy b possesses a much higher Ly $\alpha$  transmission rate as its high overdensity environment leads to a great number of bright galaxies contributing to the local ionizing photon budget, which pushes the ionizing front much further. Looking at the  $\mathcal{T}-\Delta_{3\text{D}}$  panel of Fig. 2,

<sup>4</sup> In other words, satellite galaxies (by definition) are fainter than their centrals in an ionized region with a given optical depth.

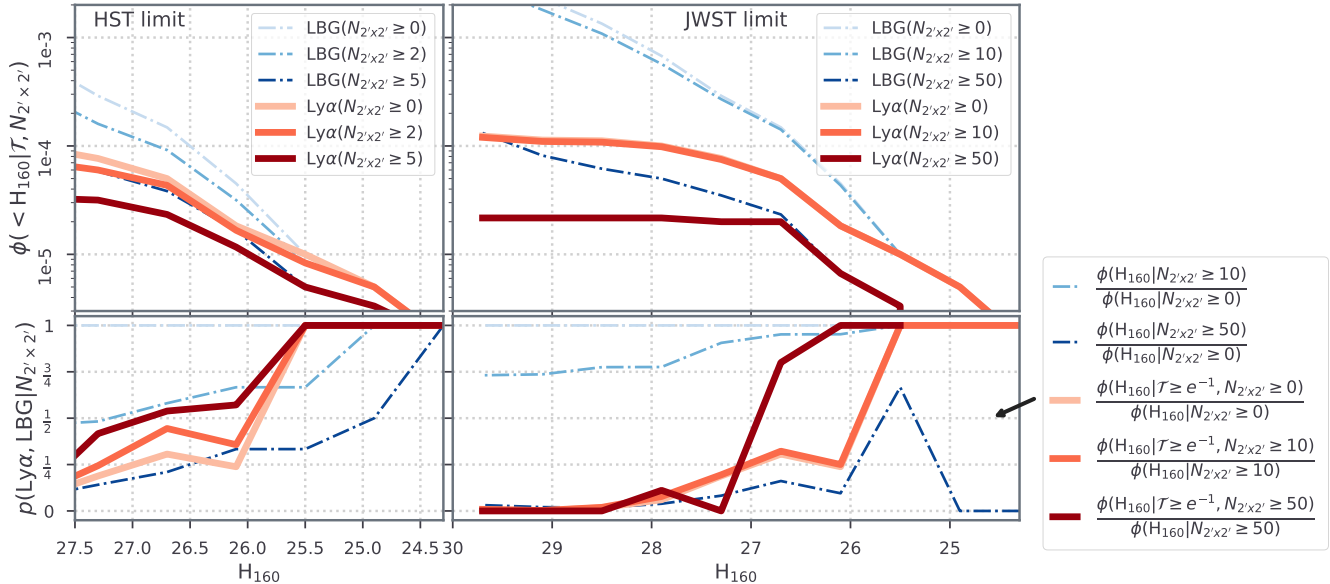


**Figure 3.** *Upper-left panel:* the cumulative number density in units of  $\text{cMpc}^{-3}\text{mag}^{-1}$  as a function of galaxy UV magnitude ( $H_{160}$ ) for all central galaxies ( $\phi(<H_{160}|N_{2' \times 2'} \geq 0$ ); light-blue dash-dotted thin line), centrals with more than 1 bright (i.e.  $H_{160} < 27.5$ ) neighbours ( $\phi(<H_{160}|N_{2' \times 2'} \geq 2$ ); medium-blue dash-dotted thin line) and with at least 5 bright neighbours ( $\phi(<H_{160}|N_{2' \times 2'} \geq 5$ ); dark-blue dash-dotted thin line) as well as central galaxies with detectable Ly $\alpha$  emission including all transparent LAEs ( $\phi(<H_{160}|\mathcal{T} \geq e^{-1}, N_{2' \times 2'} \geq 0$ ); light-red solid thick line), and those with  $\geq 2$  (i.e.  $\phi(<H_{160}|\mathcal{T} \geq e^{-1}, N_{2' \times 2'} \geq 2$ ); medium-red solid thick line) or  $\geq 5$  bright neighbouring galaxies (i.e.  $\phi(<H_{160}|\mathcal{T} \geq e^{-1}, N_{2' \times 2'} \geq 5$ ); dark-red solid thick line). *Upper-right panel:* similar to the previous panel for a typical *HST* extragalactic field, this panel forecasts for upcoming deep *JWST* surveys with the detection limit for target galaxies and their neighbours updated to  $H_{160} < 30$  and with a redshift uncertainty of  $\Delta z = 0.35$ . Note that the  $N_{2' \times 2'}$  limits are changed to  $\geq 10$  (overlapped with  $\phi(<H_{160}|\mathcal{T} \geq e^{-1}, N_{2' \times 2'} \geq 0$ )) and 50. *Lower panels:* the number density of central galaxies with varying  $N_{2' \times 2'}$  normalized by  $\phi(H_{160}|N_{2' \times 2'} \geq 0)$  (blue dash-dotted thin lines in the upper panels) as well as those with detectable Ly $\alpha$  emission normalized by the total galaxy population with corresponding  $N_{2' \times 2'}$  (see the legend in the lower-right corner for *JWST* as an example for more details).

we see that, compared to those dominating their UV background alone (empty red circles), galaxies with neighbours in their HII regions (filled red circles) are more likely to reside in high-density regions, and are less obscured by the Ly $\alpha$  damping-wing absorption.

To illustrate this in more detail, we select mock (central) galaxies brighter than  $H_{160} = 27.5$  mag and plot their Ly $\alpha$  transmission fluxes as a function of the number of neighbours (also with  $H_{160} < 27.5$  mag) in the second panel on the bottom of Fig. 2. As before, this luminosity threshold is chosen to match the current observational limit (e.g. CANDELS DEEP 5 $\sigma$  depth, see e.g. Roberts-Borsani et al. 2016) and the number count is done in a  $2' \times 2'$  FoV centred at the target object with an observational depth of  $\Delta z \sim 1$ . We see a positive correlation between  $\mathcal{T}$  and  $N_{2' \times 2'}$  – galaxies with an increasing number of neighbours are more likely to have their surrounding gas ionized to a great distance, and therefore their Ly $\alpha$  emission is less obscured by damping-wing absorption. It is worth noting that, as transparent LAEs are located in bubbles with a radius of  $\gtrsim 7\text{cMpc}$  (larger than the FoV in the mock image), their neighbouring galaxies are also likely to be observable in Ly $\alpha$ . From the second bottom panel of Fig. 2, we see that, on average,  $\gtrsim 4$  LAEs can be found in those highly ionized regions.

### 3.3 Searching for ionizing bubbles at $z \gtrsim 7$

The lower-left panel of Fig. 2 illustrates that the majority of modelled galaxies with  $H_{160} \lesssim 26$  mag have bright neigh-

bours within a WFC3 FoV. This agrees with preliminary results (Leonova et al., in prep; see also Tilvi et al. 2020) from an environmental study of 3 confirmed  $z \sim 8$  LAEs (i.e. EGS-zs8-1, EGS-zs8-2 and EGSY-z8p7; Oesch et al. 2015; Roberts-Borsani et al. 2016; Zitrin et al. 2015) – up to 6 LBGs brighter than  $H_{160} \sim 27.5$  mag were revealed in each of their *HST* WFC3 images (see the star symbols in Fig. 2). Finding more of these objects will help understand their properties and impact during the EoR, as well as to infer the ionizing bubble size and to quantify the morphology of reionization. Therefore, in this subsection, we further explore the strategy to search for LAEs during the EoR.

In the upper-left panel of Fig. 3, we present the cumulative number density,  $\phi(<H_{160})$ , for all central galaxies with a varying number of bright neighbours as well as for those classified as transparent LAEs. The fraction of modelled LBGs with detectable Ly $\alpha$  emission,  $p(\text{Ly}\alpha)$ , is an informative quantity. Not only can it place constraints on the neutral hydrogen fraction (e.g. Mesinger et al. 2015; Mason et al. 2018b), in a blind survey of Ly $\alpha$  emission among known high-redshift LBGs,  $p(\text{Ly}\alpha)$  is also an indicator of the detection rate. The lower left panel of Fig. 3 presents  $p(\text{Ly}\alpha)$  as a function of the galaxy UV luminosity and  $N_{2' \times 2'}$ , together with the fraction of LBGs having different number of neighbours for comparison.

We find that the success rate for finding LAEs among LBGs regardless of their environment is 100% when targeting the brightest galaxies (i.e.  $H_{160} \lesssim 25.5$  mag). This rate drops significantly towards the fainter end (e.g. 20 – 30%

at  $H_{160}$  between 26 and 27.5 mag). Considering only LBGs surrounded by bright neighbours can increase the detectability. For instance, at the current observing limit ( $H_{160} < 27.5$  mag), we find that following up galaxies with at least 2 neighbours can boost the detectability up to 40%. This number rises to nearly 60% when focusing on galaxies with  $\geq 5$  neighbours. However, as shown by the LBG fraction curves in Fig. 3, only  $\lesssim 25\%$  of galaxies brighter than  $H_{160} = 26$  mag have  $N_{2' \times 2'} \geq 5$  neighbours. Therefore, we conclude an optimal survey strategy for finding LAEs is to follow up with spectroscopy all LBGs brighter than  $H_{160} = 26$  mag while only focusing on fainter ones with at least 2 neighbours.

In the coming decade, *JWST* will allow study of galaxies at magnitudes much fainter than  $H_{160} = 27.5$  mag (i.e., the empty squares shown in Fig. 2). To model this we reconsider the detection threshold to be  $H_{160} = 30$  mag, and search for neighbouring galaxies that will be detectable by *JWST*. For simplicity, we use the same FoV<sup>5</sup> as the mock *HST* WFC3 survey but assume reduced photometric uncertainties and consider  $\Delta z = 0.35$  (i.e. our simulation box size). From the lower right panel of Fig. 2, we see the number of neighbours increases by a factor of  $\sim 10$  and that, on average,  $\gtrsim 25$  galaxies (which are also observable in  $\text{Ly}\alpha$ ) with  $H_{160} < 30$  mag are found in the area surrounding transparent LAEs. Consequently, we will need to target galaxies with many more neighbours to see an influence of neighbours on  $\tau$ , since  $N_{2' \times 2'} \geq 10$  is nearly identical<sup>6</sup> to  $N_{2' \times 2'} \geq 0$  (i.e. all transparent LAEs). From the right panels of Fig. 3, we find a number of  $\sim 50$  neighbours is optimal in order to reach a detection rate of  $> 50\%$  at  $H_{160} \lesssim 27$  mag. At even fainter magnitudes, the  $\text{Ly}\alpha$  emission from most galaxies will be highly attenuated by damping-wing absorption.

#### 4 CONCLUSION

In this work, we study  $\text{Ly}\alpha$  transmission in the IGM by forward-modelling the damping-wing absorption using *MERAXES*, a coupled galaxy formation and reionization SAM that is consistent with the measured high-redshift LBG luminosity functions and EoR history inferred from *Planck* (Qin et al. 2017b). As more luminous galaxies (and their neighbours) are able to ionize surrounding inter-galactic hydrogen to a much larger radius than fainter galaxies, we find the inter-galactic  $\text{Ly}\alpha$  absorption becomes weaker towards brighter galaxies. We assume the detectability of  $\text{Ly}\alpha$  to be determined by the damping-wing optical depth (hence the size of the ionized bubble in which they sit) and define LBGs with a total  $\text{Ly}\alpha$  optical depth less than 1 to be transparent LAEs. Our model shows that transparent LAEs will be found in HII bubbles that are at least 7cMpc in size at  $z = 8$  (where the global neutral hydrogen fraction is predicted to be  $\sim 86\%$ ).

<sup>5</sup> With NIRCcam, *JWST* observes two areas of  $2.2' \times 2.2'$  FoV separated by a gap of  $\sim 0.7'$ .

<sup>6</sup> The *JWST* NIRCcam grism programs (e.g. Malkan et al. 2021; Naidu et al. 2021; Oesch et al. 2021) will obtain 3D information and therefore the spatial correlation will become much improved from better redshift resolution. However, in this case, even with our reduced redshift uncertainties ( $\Delta z = 0.35$ ), we may be still overestimating the foreground/background sources.

In particular, we find that all modelled LBGs with  $H_{160} \lesssim 25.5$  mag are detectable LAEs. This is consistent with the high detection rate (i.e.  $p(\text{Ly}\alpha) = 100\%$ ) of  $\text{Ly}\alpha$  emission in recent spectroscopic follow-up of the 4 brightest galaxies at  $z \sim 8$  (Oesch et al. 2015; Zitrin et al. 2015; Roberts-Borsani et al. 2016; Stark et al. 2017; Tilvi et al. 2020). These results, in addition to the more recent findings of  $z \sim 8$  LAEs by Jung et al. (2020); Endsley et al. (2021) and Laporte et al. (2021) indicate very high LAE fractions among luminous galaxies beyond  $z \sim 6$ . This is in contrast to measurements of fainter galaxies in deep fields or using less-massive lensed galaxies, which show a significant drop of  $p(\text{Ly}\alpha)$  from  $z = 6$  to 8 (Schenker et al. 2014; Hoag et al. 2019). Our simulation (see Fig. 1) suggests that the combination of these measurements at both high and low luminosity provides evidence for massive LAEs being likely to reside in large HII bubbles.

We also find that reionization is more advanced around galaxies in high-density regions compared to those that are isolated, with galaxies having a larger number of bright neighbours being more likely to reside in large HII bubbles, leading to  $\text{Ly}\alpha$  emission that is less attenuated by the IGM. This not only provides evidence that overdensity plays an important role in driving reionization, but can also motivate searching for LAEs in high-density environments during reionization. Transparent LAEs, on average, are located in overdense regions and are found to possess  $\gtrsim 2(25)$  neighbouring galaxies brighter than  $H_{160} \sim 27.5(30)$  mag within mock images of  $2' \times 2'$  FoV. As their neighbours are also within the same HII bubbles, they are also likely to be observable in  $\text{Ly}\alpha$ .

Finding more high-redshift LAEs will help quantify the morphology of the EoR and infer the properties of galaxies responsible for driving the reionization. We find that while nearly 70–80% of  $z = 8$  galaxies with  $H_{160}$  between 26 and 27.5 mag experience strong damping-wing absorption, targeting those surrounded by bright neighbours can significantly increase the incidence of  $\text{Ly}\alpha$  emission. For example, at the current observational limit, 40% galaxies with more than 1 neighbour would be considered detectable LAEs. This number increases to 60% when focusing on galaxies with at least 5 neighbours. Finally, we predict that upcoming *JWST* observations are likely to reveal a factor of 10 more neighbouring galaxies. With such a large sample size, we find that targeting galaxies with  $\sim 50$  neighbours will yield a success rate of more than 50% for finding LAEs among LBGs during the EoR. These large samples from *JWST* will provide insights into the morphology and scale sizes of the ionized regions, and their development and growth with redshift through the EoR, that is just not possible with *HST*.

#### ACKNOWLEDGEMENTS

This research was supported by the Australian Research Council Centre of Excellence for All Sky Astrophysics in 3 Dimensions (ASTRO 3D), through project #CE170100013. Parts of this work was supported by the European Research Council (ERC) under the European Union’s Horizon 2020 research and innovation programme (AIDA – #638809). The results presented here reflect the authors’ views; the ERC is not responsible for their use. The simulations presented in this work were run on the OzSTAR national facility at Swin-



burne University of Technology. PAO acknowledges support from the Swiss National Science Foundation through the SNSF Professorship grant 190079. The Cosmic Dawn Center (DAWN) is funded by the Danish National Research Foundation under grant No. 140. GDI is grateful for support from program HST-GO-15103.002-A from STScI/AURA Inc under NASA contract NAS 5-26555. RPN gratefully acknowledges an Ashford Fellowship granted by Harvard University.

## DATA AVAILABILITY

The data underlying this article will be shared on reasonable request to the corresponding author.

## REFERENCES

- Bañados E. et al., 2018, *Nature*, 553, 473
- Becker G. D., Bolton J. S., Madau P., Pettini M., Ryan-Weber E. V., Venemans B. P., 2015, *MNRAS*, 447, 3402
- Bolton J. S., Becker G. D., Wyithe J. S. B., Haehnelt M. G., Sargent W. L. W., 2010, *MNRAS*, 406, 612
- Bolton J. S., Puchwein E., Sijacki D., Haehnelt M. G., Kim T.-S., Meiksin A., Regan J. A., Viel M., 2017, *MNRAS*, 464, 897
- Bongiorno A. et al., 2007, *Astronomy & Astrophysics*, 472, 443
- Bosman S., 2020, All  $z > 5.7$  quasars currently known
- Bouwens R. J. et al., 2015, *ApJ*, 803, 34
- Bouwens R. J. et al., 2016, *ApJ*, 830, 67
- Chardin J., Haehnelt M. G., Aubert D., Puchwein E., 2015, *MNRAS*, 453, 2943
- Chardin J., Puchwein E., Haehnelt M. G., 2017, *MNRAS*, 465, 3429
- Choudhury T. R., Puchwein E., Haehnelt M. G., Bolton J. S., 2015, *MNRAS*, 452, 261
- Croom S. M. et al., 2009, *MNRAS*, 399, 1755
- D’Aloisio A., McQuinn M., Davies F. B., Furlanetto S. R., 2018, *MNRAS*, 473, 560
- D’Aloisio A., McQuinn M., Trac H., 2015, *ApJ*, 813, L38
- Davies F. B., Furlanetto S. R., 2016, *MNRAS*, 460, 1328
- Davies F. B. et al., 2018, *ApJ*, 864, 142
- Davies J. E., Croft R. A. C., Di-Matteo T., Greig B., Feng Y., Wyithe J. S. B., 2021, *MNRAS*, 501, 146
- Dijkstra M., 2014, *PASA*, 31, e040
- Dijkstra M., Lidz A., Wyithe J. S. B., 2007, *MNRAS*, 377, 1175
- Endsley R., Stark D. P., Charlot S., Chevallard J., Robertson B., Bouwens R. J., Stefanon M., 2021, *MNRAS*, 502, 6044
- Erb D. K. et al., 2014, *ApJ*, 795, 33
- Fontana A. et al., 2010, *ApJ*, 725, L205
- Furlanetto S. R., Zaldarriaga M., Hernquist L., 2004, *ApJ*, 613, 1
- Gaikwad P. et al., 2020, *MNRAS*, 494, 5091
- Garel T., Blaizot J., Guiderdoni B., Michel-Dansac L., Hayes M., Verhamme A., 2015, *MNRAS*, 450, 1279
- Garel T., Blaizot J., Rosdahl J., Michel-Dansac L., Haehnelt M. G., Katz H., Kimm T., Verhamme A., 2021, *MNRAS*, 504, 1902
- Geil P. M., Mutch S. J., Poole G. B., Duffy A. R., Mesinger A., Wyithe J. S. B., 2017, *MNRAS*, 472, 1324
- Glikman E., Djorgovski S. G., Stern D., Dey A., Jannuzi B. T., Lee K.-S., 2011, *The Astrophysical Journal*, 728, L26
- Greig B., Mesinger A., Bañados E., 2019, *MNRAS*, 484, 5094
- Greig B., Mesinger A., Haiman Z., Simcoe R. A., 2017, *MNRAS*, 466, 4239
- Gronke M. et al., 2020, arXiv e-prints, arXiv:2004.14496
- Hassan S., Gronke M., 2021, *ApJ*, 908, 219
- Hoag A. et al., 2019, *ApJ*, 878, 12
- Hu W. et al., 2021, *Nature Astronomy*, 5, 485
- Jung I. et al., 2020, *ApJ*, 904, 144
- Keating L. C., Puchwein E., Haehnelt M. G., 2018, *MNRAS*, 477, 5501
- Keating L. C., Weinberger L. H., Kulkarni G., Haehnelt M. G., Chardin J., Aubert D., 2020, *MNRAS*, 491, 1736
- Kulkarni G., Keating L. C., Haehnelt M. G., Bosman S. E. I., Puchwein E., Chardin J., Aubert D., 2019, *MNRAS*, 485, L24
- Laporte N., Meyer R. A., Ellis R. S., Robertson B. E., Chisholm J., Roberts-Borsani G. W., 2021, *MNRAS*, 505, 3336
- Le Delliou M., Lacey C. G., Baugh C. M., Morris S. L., 2006, *MNRAS*, 365, 712
- Lee K.-G. et al., 2015, *ApJ*, 799, 196
- Lidz A., Faucher-Giguère C.-A., Dall’Aglia A., McQuinn M., Fechner C., Zaldarriaga M., Hernquist L., Dutta S., 2010, *ApJ*, 718, 199
- Liu C., Mutch S. J., Angel P. W., Duffy A. R., Geil P. M., Poole G. B., Mesinger A., Wyithe J. S. B., 2016, *MNRAS*, 462, 235
- Malkan M. A. et al., 2021, *PASSAGE-Parallel Application of Slitless Spectroscopy to Analyze Galaxy Evolution. JWST Proposal. Cycle 1*
- Mason C. A. et al., 2018a, *ApJ*, 857, L11
- Mason C. A., Treu T., Dijkstra M., Mesinger A., Trenti M., Pentericci L., de Barros S., Vanzella E., 2018b, *ApJ*, 856, 2
- Masters D. et al., 2012, *The Astrophysical Journal*, 755, 169
- McGreer I. D., Mesinger A., D’Odorico V., 2015, *MNRAS*, 447, 499
- Meiksin A., 2020, *MNRAS*, 491, 4884
- Mesinger A., Aykutalp A., Vanzella E., Pentericci L., Ferrara A., Dijkstra M., 2015, *MNRAS*, 446, 566
- Mesinger A., Furlanetto S., Cen R., 2011, *MNRAS*, 411, 955
- Miralda-Escudé J., 1998, *ApJ*, 501, 15
- Mortlock D. J. et al., 2011, *Nature*, 474, 616
- Murray S., Greig B., Mesinger A., Muñoz J., Qin Y., Park J., Watkinson C., 2020, *The Journal of Open Source Software*, 5, 2582
- Mutch S. J., Geil P. M., Poole G. B., Angel P. W., Duffy A. R., Mesinger A., Wyithe J. S. B., 2016, *MNRAS*, 462, 250
- Mutch S. J. et al., 2016, *MNRAS*, 463, 3556
- Muzahid S. et al., 2020, *MNRAS*, 496, 1013
- Naidu R. et al., 2021, *Where Cosmic Dawn Breaks First: Mapping the Primordial Overdensity Powering a  $z \approx 9$  Ionized Bubble. JWST Proposal. Cycle 1*

- Nasir F., D'Aloisio A., 2020, *MNRAS*, 494, 3080
- Oesch P. et al., 2021, *FRESCO: The First Reionization Epoch Spectroscopic COmplete Survey*. JWST Proposal. Cycle 1
- Oesch P. A. et al., 2015, *ApJ*, 804, L30
- Ono Y. et al., 2012, *ApJ*, 744, 83
- Oyarzún G. A., Blanc G. A., González V., Mateo M., Bailey, John I. I., 2017, *ApJ*, 843, 133
- Palanque-Delabrouille N. et al., 2013, *A&A*, 551, A29
- Park H. et al., 2021, *arXiv e-prints*, arXiv:2105.10770
- Planck Collaboration et al., 2016, *A&A*, 594, A13
- Planck Collaboration et al., 2020, *A&A*, 641, A6
- Poole G. B., Angel P. W., Mutch S. J., Power C., Duffy A. R., Geil P. M., Mesinger A., Wyithe S. B., 2016, *MNRAS*, 459, 3025
- Puchwein E., Bolton J. S., Haehnelt M. G., Madau P., Becker G. D., Haardt F., 2015, *MNRAS*, 450, 4081
- Qin Y., Mesinger A., Bosman S. E. I., Viel M., 2021, *MNRAS*, 506, 2390
- Qin Y., Mutch S. J., Duffy A. R., Geil P. M., Poole G. B., Mesinger A., Wyithe J. S. B., 2017a, *MNRAS*, 471, 4345
- Qin Y. et al., 2017b, *MNRAS*, 472, 2009
- Qin Y., Poulin V., Mesinger A., Greig B., Murray S., Park J., 2020, *MNRAS*, 499, 550
- Roberts-Borsani G. W. et al., 2016, *ApJ*, 823, 143
- Schenker M. A., Ellis R. S., Konidaris N. P., Stark D. P., 2014, *ApJ*, 795, 20
- Song H., Seon K.-I., Hwang H. S., 2020, *ApJ*, 901, 41
- Stark D. P. et al., 2017, *MNRAS*, 464, 469
- Stark D. P., Ellis R. S., Chiu K., Ouchi M., Bunker A., 2010, *MNRAS*, 408, 1628
- Tilvi V. et al., 2020, *ApJ*, 891, L10
- Trac H. Y., Gnedin N. Y., 2011, *Advanced Science Letters*, 4, 228
- Treu T., Schmidt K. B., Trenti M., Bradley L. D., Stiavelli M., 2013, *ApJ*, 775, L29
- Verhamme A., Schaerer D., Maselli A., 2006, *A&A*, 460, 397
- Wang F. et al., 2020, *ApJ*, 896, 23
- Wolf C., Wisotzki L., Borch A., Dye S., Kleinheinrich M., Meisenheimer K., 2003, *A&A*, 408, 499
- Wyithe J. S. B., Loeb A., 2005, *ApJ*, 625, 1
- Yang H. et al., 2017, *The Astrophysical Journal*, 844, 171
- Yang J. et al., 2020, *ApJ*, 897, L14
- Zheng Z., Cen R., Trac H., Miralda-Escudé J., 2010, *ApJ*, 716, 574
- Zitrin A. et al., 2015, *ApJ*, 810, L12